



Effect of PANI on the structural, optical and electrical properties of PMMA/PEO blended polymers loaded with $\text{CuCo}_2\text{O}_4/\text{MnS}$ nanocomposite

A. M. El-naggar¹ · A. M. Kamal² · A. A. Albassam¹

Received: 5 August 2023 / Accepted: 18 September 2023 / Published online: 7 October 2023
© The Author(s), under exclusive licence to Springer Science+Business Media, LLC, part of Springer Nature 2023

Abstract

Poly(methyl methacrylate/poly(ethylene oxide) (PMMA/PEO)/(1-x) CuCo_2O_4 /xMnS blends with and without polyaniline (PANI) were prepared using hydrothermal, solid-state reaction and casting procedures. X-ray diffraction (XRD) and the transmission electron microscope techniques were applied to explore the different phases in the nanocomposite and their crystallite sizes. XRD explored the effect of nanocomposite doping on the formed blends with and without PANI. The absorption, transmittance, reflectance, extinction coefficient, optical dielectric constant, energy loss functions and optical conductivity for PMMA/PEO/(1-x) CuCo_2O_4 /xMnS blends with and without PANI were studied using the diffused reflectance technique. The values for PMMA/PEO's direct and indirect optical band gap (E_g) are 5.06 and 4.79 eV, respectively. As 50% MnS and PANI were present in the blend loaded with nanocomposite, the direct/indirect E_g (4.89/4.49) eV values were achieved. At 500 nm, the refractive index of the blend was increased from 1.37 to 1.48 as it doped with 0.5 CuCo_2O_4 /0.5MnS. The effect of (1-x) CuCo_2O_4 /xMnS and PANI on the fluorescence spectra of the PMMA/PEO blend was investigated. Blends exhibited varying degrees of bluish-violet color. The AC conductivity and the energy density were explored. Doping the blend with nanocomposite samples and PANI resulted in a lower energy density, with the exception of the blend containing 50% MnS and PANI, where it rose. The doped blends that were studied could be used in photocatalytic reactions.

Keywords PMMA · $\text{CuCo}_2\text{O}_4/\text{MnS}$ nanocomposite · PANI · Structure · Optical · Electrical

✉ A. M. El-naggar
elnaggar@ksu.edu.sa

A. M. Kamal
amgadmazhar@yahoo.com

A. A. Albassam
aabassam@ksu.edu.sa

¹ Research Chair of Exploitation of Renewable Energy Applications in Saudi Arabia, Physics and Astronomy Department, College of Science, King Saud University, P.O. Box 2455, 11451 Riyadh, Saudi Arabia

² Physics and Astronomy Department, College of Science, King Saud University, P.O. Box 2455, 11451 Riyadh, Saudi Arabia

1 Introduction

Blended polymer composites with desirable optical features are essential for the development of materials for uses in optical communication, optical sensors, solar cells, light-emitting diodes, polarizers, data storage devices, and the biomedical sector, among others. The potential applications of polymer/inorganic nanocomposites in optoelectronic devices have attracted commercial interest in the incorporation of inorganic nanoparticles into polymers. Nanofillers are widely used in polymers to boost their optical and electrical properties (El-naggar et al. 2023a, b, c). Polymethyl methacrylate (PMMA) is widely recognized as a superior optical polymer. Its visible light transmission rate is 92%, which is better than glass (Wu et al. 2022). Polyethylene oxide (PEO) has a linear structure that owns semicrystalline polymer that includes crystalline and amorphous phases at ambient temperature; nevertheless, it exhibits a crystalline structure in its pure form. Due to their relatively high thermal stability, PEO-based materials are favorable polymer candidates (Abdelrazek et al. 2017). It possesses a number of desirable properties, including adequate corrosion resistance, cost-effectiveness, good conductivity in the amorphous structure and satisfactory dimensional stability; however, it has a relatively low index of refractive (Ngai et al. 2016; Mathela et al. 2022). Polyaniline (PANI) is the most remarkable and studied polymer among all conducting polymers because it can be synthesized cheaply, has reasonable conductivity, redox features, and good environmental stability, and is gaining additional interest due to its potential applications in the fields of anti-corrosion coatings, electrochromic devices, electrode substantial in batteries and supercapacitors, light-emitting diodes, chemical sensors, and bifunctional materials (Naidu and Palaniappan 2020).

As the polymer or blend is loaded with the right dopants, its properties will change. For example, CaTiO₃ nanoparticles embedded in PEO have found applications in optoelectronics (Aziz et al. 2021). Sodium alginate/polyvinyl alcohol/zinc oxide/iron oxide nanocomposites were used in the electrochemical applications (Albalawi et al. 2023). Farea et al. (2022) found high performance in carbon monoxide gas sensors based on a novel poly(3,4-ethylenedioxythiophene)-poly(styrenesulfonate)/poly(p-anisidine) nanocomposite. Laser-etched of the novel ternary nanocomposite of poly (ethylmethacrylate)/polystyrene/silver nanoparticles films exhibit improved electrical conductivity and dielectric performance (El-Sharnouby et al. 2022). The electrical conductivity results showed that increasing the selenium nanoparticle amounts in PEO/Cs enhanced the dielectric behavior of the PEO/Cs/Se NPs films (Alzahrani et al. 2022a).

Polyaniline/poly (vinyl acetate) composites are a promising new material for employ in a widespread range of optoelectronic devices because of their improved optical and electrical properties (Wadatkar and Waghuley 2021). PVA/PANI/Ag nanocomposite films were identified as a new and talented material for optoelectronic uses by Abdelhamied et al. (2020). Doping polyethylene oxide and polyacrylamide: Li polymer electrolyte films with Ag nanoparticles improved their optical, thermal, and electrical features (Morsi et al. 2018). The PMMA matrix doped with wide bandgap metal oxide semiconductors (ZnO, SnO₂, and TiO₂ nanocrystallites) shows great promise for use in future generations of a wide variety of optoelectronic, organo-electronic, and microelectronic devices (Sengwa 2021).

Capacitive energy storage utilizing polymer dielectrics has seen widespread use. However, polymer dielectrics generally have a low volumetric energy density, which falls short of the requirements for high-power and compact-size electronic devices and electrical systems (Wang et al. 2022). In order to achieve a high breakdown strength

and charge discharge efficiency, polymers and nanoparticles are combined and used, which takes advantage of the high insulation properties of nanoparticles (Yang et al. 2022). By varying the SnO₂ contents, it is possible to adjust the real part of the (PEO-PMMA)-*x* wt% SnO₂ films' dielectric permittivity. In order to design flexible type microelectronic devices, a polymeric nanodielectric substrate with a low permittivity, such as (PEO-PMMA)-*x* wt% SnO₂, is formed (Choudhary 2017). High discharge energy density and charge discharge efficiency are observed in poly(vinylidene fluoride-co-hexafluoropropylene)/a-SiO₂ (Yang et al. 2022).

Cobaltite, such as CuCo₂O₄, a transition metal, is crucial component used in numerous applications (Heiba et al. 2021a; Liu et al. 2022). Two direct band gaps (1.43 and 2.05 eV) were observed in CuCo₂O₄ thin film (McLure 1957), while one optical band gap (4.02 eV) was observed in CuCo₂O₄ synthesized using a one-step chemical route (Koninck et al. 2006).

The semiconductor manganese sulphide (MnS) has a large optical band gap of about 3 eV (Heiba et al. 2021b; Pei et al. 2019). The rock-salt-structured, high-temperature-prepared- α -MnS is the most stable form of MnS. Both the tetrahedral β -phase and the hexagonal γ -phase, which are metastable phases, were prepared at low temperatures (Heiba et al. 2021c). As the MnS content of the nanocomposite grew in the (1-*x*) CuCo₂O₄/*x*MnS nanocomposite, there was noticeable variation in the position of the two indirect optical band gaps of pure CuCo₂O₄. With *x*=0.5, the optical parameters of the (1-*x*) CuCo₂O₄/*x*MnS nanocomposite are enhanced (Heiba et al. 2022).

In this work, (1-*x*)CuCo₂O₄/*x*MnS samples were prepared via hydrothermal and solid state reaction methods. Undoped and doped PMMA/PEO blends with (1-*x*) CuCo₂O₄/*x*MnS and/or PANI were fabricated using the casting method. The effect of the fillers on the structural, dielectric properties, electric modulus, ac conductivity and energy density of the PMMA/PEO blend were examined using an LCR meter device. The behaviors of linear and nonlinear optical parameters of the PMMA/PEO blend were also explored upon doping with different fillers.

2 Methods and materials

2.1 Preparation of the nanocomposite samples

Under magnetic stirring for 30 min, (copper and cobalt) nitrates and urea were dissolved in deionized water (35 ml) to create nano CuCo₂O₄. The resulting solution was moved to a Teflon-lined stainless-steel autoclave and heated for 24 h at 120 °C. Once the autoclave reached room temperature (*RT*), the process was complete. The resulting solution experienced repeated centrifugation and washing with deionized water and ethanol. The manufactured powder was subsequently dried and annealed in a 350 °C (1 h) electric oven. To make (1-*x*)CuCo₂O₄/*x*MnS (*x*=0.25, 0.5), first manganese acetate and thiourea were dissolved in 10 ml of deionized water at a stoichiometric ratio (1:1) to create MnS nanoparticles in the presence of CuCo₂O₄ nanoparticles.

To prevent MnS from being oxidized, the solution was annealed at 250 °C (2 h) after being stirred on a magnetic stirrer for 30 min.

2.2 Preparation of the undoped and doped blends:

Using the casting technique, we were able to create an undoped blend of 50% wt% PMMA and 50% wt% PEO by dissolving 1 g of poly(methyl methacrylate, PMMA, sigma Aldrich) and 1 g of poly(ethylene oxide, PEO, sigma Aldrich) separately in 20 ml of chloroform at RT . Then, for 12 h at RT , the two solutions were mixed together. These steps were repeated with 3 wt% $(1-x)$ $CuCo_2O_4/xMnS$ present. The former steps were repeated to form PMMA/PEO/ $(1-x)CuCo_2O_4/xMnS$ with PANI as follows: 0.1 wt% polyaniline (PANI, Sigma Aldrich) was added to the above solution and it dissolved using ultrasonicators for 5 h at RT . The resulting solutions were transferred to a Petri dish and then heated in an oven at RT for 1 day.

The thickness of the resulting blends, measured with a digital micrometer accurate to within $\pm 10 \mu m$, is between 240 and 270 μm .

2.3 Apparatus and luminescence

An X-ray diffractometer (PANalytical diffractometer, X'pert MPD, Philips, copper source) was employed to examine all of the nanocomposite fillers and blends. The nano-size range of the samples was analyzed using the high-resolution transmission electron microscope (TEM, JEOL JEM-2100, 200 kV). A diffuse reflectance spectrophotometer (JASCO-V-670, coupled to an integrating sphere assembly) was utilized to collect data on the UV diffuse reflectance (R) and transmittance (T) of all blends. The following is used to correct the R value (El-naggar et al. 2023d):

$$R_i = \frac{[2 + T^2 - (1 - R)^2] - \left\{ [2 + T^2 - (1 - R)^2]^2 - 4(2 - R)R \right\}^{0.5}}{2(2 - R)} \quad (1)$$

$$R_F = \left(2 + T^2 - (1 - R_i)^2 - \left\{ [2 + T^2 - (1 - R_i)^2]^2 - 4R_i(2 - R_i) \right\}^{0.5} \right) (2(2 - R_i))^{-1} \quad (2)$$

where R_i and R_F are the interface reflectance and reflection from one face, respectively.

The following relations were used to determine the corrected absorbance ($A_{corrected}$), refractive index (n), and extinction coefficient (k) of each blend (El-naggar et al. 2023d):

$$A_{corrected} = \ln\left(\frac{R_F T}{R_i - R_F}\right) \quad (3)$$

$$k(R_i, T) = \frac{\lambda}{4\pi d} \ln \left[\frac{R_F(R_i, T)T}{R_i - R_F(R_i, T)} \right] \quad (4)$$

$$n = \frac{1 + R_F(R_i, T)}{1 - R_F(R_i, T)} + \left\{ \frac{4R_F(R_i, T)}{(1 - R_F(R_i, T))^2} - \left(\frac{\lambda}{4\pi d}\right)^2 \ln^2 \left[\frac{R_F(R_i, T)T}{R_i - R_F(R_i, T)} \right] \right\}^{0.5} \quad (5)$$

Using a luminescence spectrophotometer (FP-8200 JASCO), we were able to acquire fluorescence (FL) spectra. The dielectric constant parameters as a function of frequency at RT are obtained by applying a 2 V ac voltage and measuring the resulting changes in capacitance (C) and dissipation factor ($\tan \delta$) with a GWINSTEK LCR 8105G device.

Each blend's ac conductivity (σ_{ac}), dielectric constant (ϵ' , ϵ''), and complex electric modulus ($M^* = M' + iM''$) were calculated using the equations listed below (Heiba et al. 2023):

$$\epsilon' = dC/\epsilon_0 A \quad (6)$$

$$\sigma_{ac} = 2\pi f \epsilon_0 \epsilon' \tan \delta \quad (7)$$

$$\tan \delta = \epsilon''/\epsilon' \quad (8)$$

$$M' = \frac{\epsilon'}{\epsilon'^2 + \epsilon''^2} \quad (9)$$

$$M'' = \frac{\epsilon''}{\epsilon'^2 + \epsilon''^2} \quad (10)$$

where ϵ_0 , t and A are the permittivity of free space, thickness and area of the disk, respectively.

3 Results and discussion

3.1 Structural investigation

3.1.1 Structural investigation of the nanocomposite samples

Phase identification analysis of $(1-x)\text{CuCo}_2\text{O}_4/x\text{MnS}$ nanocomposite samples showed that all samples consisted of a single phase of CuCo_2O_4 with a cubic spinel structure (Fig. 1a). As a result, Mn and S ions are implanted into the CuCo_2O_4 lattice rather than forming a MnS phase (Heiba et al. 2022). The transmission electron microscope (TEM) image of the $0.5\text{CuCo}_2\text{O}_4/0.5\text{MnS}$ sample is shown in Fig. 1b. Particles with a narrow size distribution were depicted in the figures as being nanosized. The Scherrer formula can be applied to determine the crystallite size (D) of nanocomposite samples (Abdel-Kader et al. 2023):

$$D = \frac{0.9\lambda}{\beta \cos \theta} \quad (11)$$

where λ and β are the wavelength of the X-ray technique and the full width at half maximum intensity, respectively.

3.1.2 Structural investigation of the blends

Nearly all samples have roughly the same average crystallite size, which is 15 nm. The PMMA/PEO/ $(1-x)\text{CuCo}_2\text{O}_4/x\text{MnS}$ diffraction patterns with and without PANI are shown

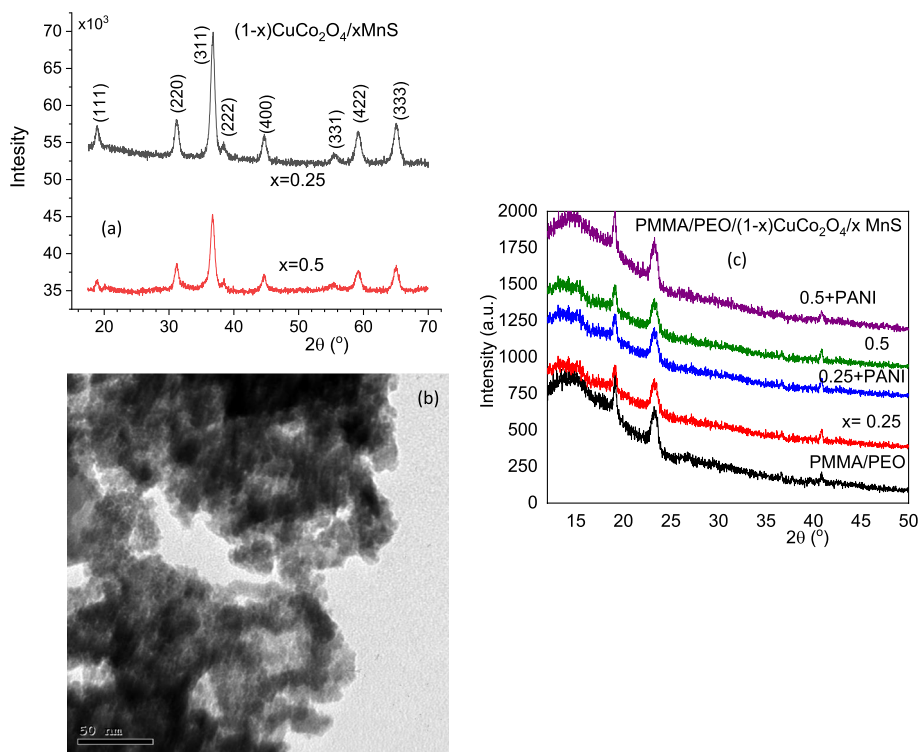


Fig. 1 **a** XRD data for $(1-x)\text{CuCo}_2\text{O}_4/x\text{MnS}$ samples, **b** TEM image for $0.75\text{CuCo}_2\text{O}_4/0.25\text{MnS}$ sample and **c** PMMA/PEO/ $(1-x)\text{CuCo}_2\text{O}_4/x\text{MnS}$ polymers with and without PANI

in Fig. 1c. As revealed from the plot. The two well-resolved diffraction peaks typical of the PEO crystalline structure are superimposed on a high background due to diffuse scattering (Pereira et al. 2011). The peak at $2\theta=19.3^\circ$ represented the crystallographic plane (120), while the peak at $2\theta=23.4^\circ$ corresponds to several planes: (032), (132), (112), (212), (004), and (124) (Burba et al. 2007). Because of the nanofiller's small concentration, no obvious peaks could be traced back to it. Also, there was no detectable PANI peak due to the low PANI concentration and high homogeneity.

3.2 Optical features

3.2.1 Optical absorption, transmittance and reflectance of the blends

Understanding the variations within the band gap range requires an investigation into the optical parameters that depend on absorption, transmission and reflectance data. The optical absorption, transmittance and reflectance data for PMMA/PEO/ $(1-x)\text{CuCo}_2\text{O}_4/x\text{MnS}$ blends with and without PANI are represented in Fig. 2. Doping the PMMA/PEO blend with $(1-x)\text{CuCo}_2\text{O}_4/x\text{MnS}$, as shown in Fig. 2a, increased the blend's absorbance. Adding more MnS to the nanocomposite also increased its absorbance. The blends' absorbance was also improved by PANI doping compared to blends without PANI. All blends have an absorption band at 233 nm, which can be attributed to C=O and/or C=C

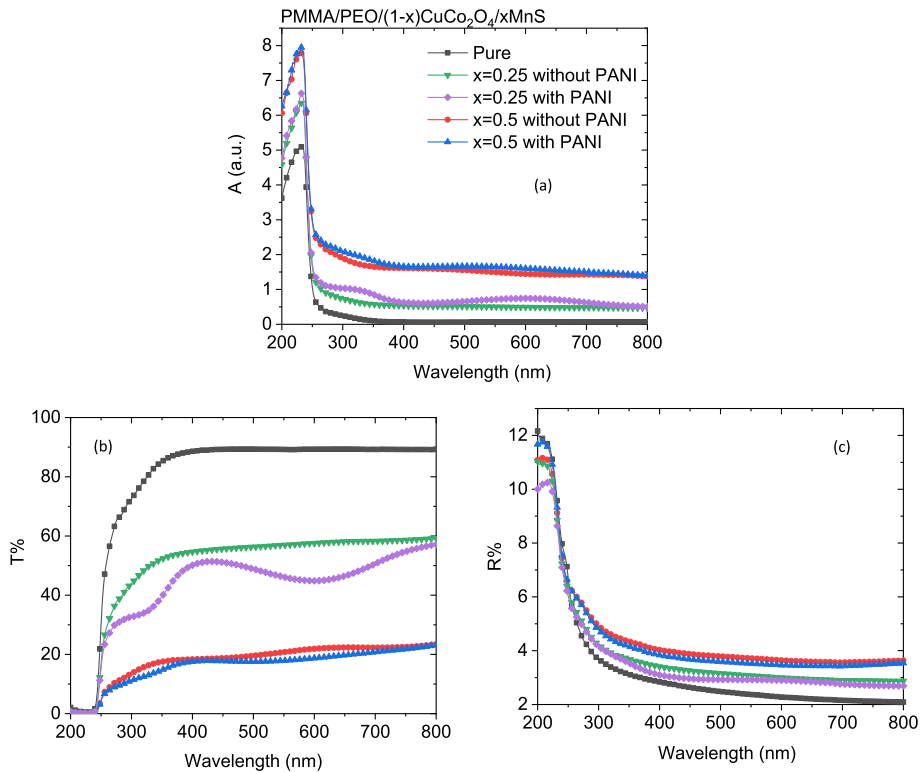


Fig. 2 **a** Absorbance, **b** transmittance and **c** reflectance spectra for PMMA/PEO/(1-x)CuCo₂O₄/xMnS polymers with and without PANI

bonds (Abutalib and Rajeh 2020). An additional $\pi-\pi^*$ transition (benzenoid and quinoid units) and polaron band can be seen in the absorbance of PMMA/PEO/(1-x)CuCo₂O₄/xMnS doped with PANI at around 325 and 605 nm, respectively (Mirmohseni and Wallace 2003; Laourari et al. 2022). Additionally, Fig. 2b shows that PMMA/PEO has a visible-range transmittance of roughly 89%. When the blend was loaded with a nanocomposite that consisted of 50% MnS and PANI, the transmittance dropped to 18%. Doping a PMMA/PEO blend with MnS led to increased reflectance in the visible spectrum, while loading the blend with PANI in addition decreased the reflectance. The packing density of the blend, and thus its reflectance behavior, can be changed by doping it with the nanocomposite and/or PANI (Kafashan et al. 2016).

3.2.2 Optical band gaps of the blends

The energy difference between the highest occupied molecular orbital (HOMO) and the lowest unoccupied molecular orbital (LUMO) can be calculated by analyzing absorption data near the absorption edge for each blend. Tauc's formula (El-naggar et al. 2023a, b, c) can be employed to find out the direct/indirect optical band gap values for any blend:

$$\alpha h\nu = D(h\nu - E_g)^r \tag{12}$$

$$\alpha = 2.303A/d \tag{13}$$

where h, ν, D, d and α are Planck’s constant, the frequency of the incident light, a constant, the thickness of the blends and the absorption coefficient, respectively. r could be 0.5 or 2 for direct or indirect transitions, respectively.

Extrapolating the linear portion to the intercept with the x-axis in Fig. 3a, b yields the direct or indirect optical band gap (E_g) energies for PMMA/PEO/(1-x) CuCo₂O₄/xMnS blends with and without PANI. The values for PMMA/PEO’s direct and indirect E_g are 5.06 and 4.79 eV, respectively, as shown in the table. Additionally, as the quantity of MnS in the nanocomposite increased, these values reduced even more. These values also decreased as the blend was doped with nanocomposite, and they decreased even more as PANI was added. As 50% MnS and PANI were present in the blend loaded with nanocomposite, the direct/indirect E_g (4.89/4.49) eV values were achieved. Nanocomposite blends of polyvinyl alcohol and carboxymethyl cellulose that were doped with niobium carbide showed comparable outcomes (Hashim and Hadi 2018). Also as poly(vinyl chloride) was doped by nanomaterials of CuO and CoO with various concentration ratios or aromatic organosilicon (Abed and Abed 2022; Abed et al. 2022). As the ratio of nanocomposite to PANI varied, so did the degree of disorder and the number of defects in the host blend, which ultimately led to this decline. As a result, the state generated locally within the optical band gap changed.

Fig. 3 Tauc relation for **a** direct and **b** indirect optical band gaps for PMMA/PEO/(1-x)CuCo₂O₄/xMnS polymers with and without PANI

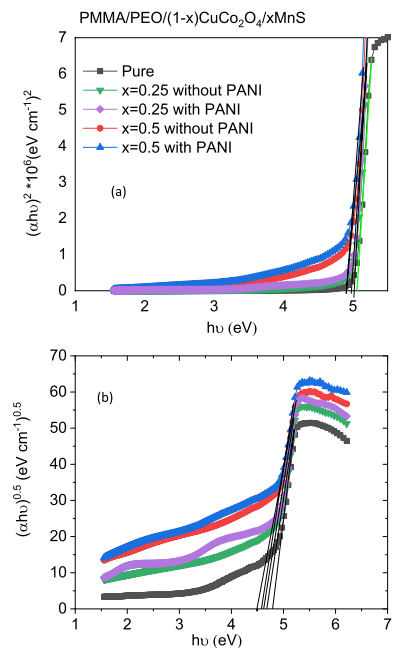
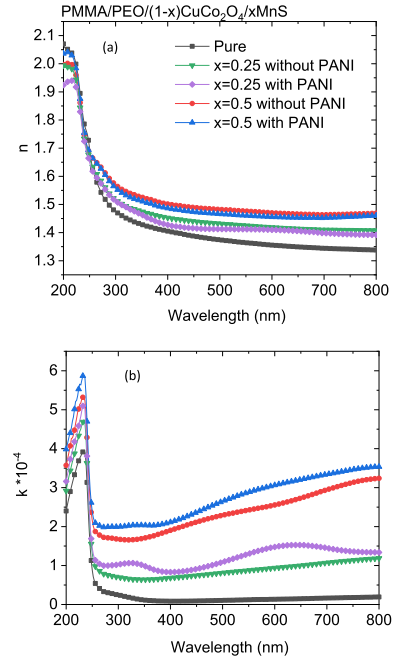


Fig. 4 **a** Refractive index and **b** extinction coefficient as function of the wavelength for PMMA/PEO/(1-x)CuCo₂O₄/xMnS polymers with and without PANI



3.2.3 Refractive index and extinction coefficient of the blends

As revealed from Fig. 4a, the refractive indices (n) for both undoped and doped PMMA/PEO blends exhibited a normal dispersion, where n values reduced as the wavelength raised. Doping the blend led to an increase in its n value relative to the undoped blend. As the quantity of MnS in the nanocomposite rose, the n value of the doped blend increased, but it reduced in the corresponding blend with PANI. Similar results were detected in polyvinyl chloride doped with nano chromium (III) oxide (Abed et al. 2021a). It has been shown that doping a blend with a nanocomposite/PANI can change the n value of the blend, which in turn can change the density of chain packing (El-Shamy 2021). The extinction coefficient (k) values also increased with (1-x) CuCo₂O₄/xMnS loading and increased further with PANI doping (Fig. 4b). When more MnS was incorporated into the nanocomposite, the value of k rose. Similar results were detected as poly(vinyl chloride) film exposure to light (Abed et al. 2021b). The existence of fillers in blends may account for the change in k value seen after doping (Tanaka 1980), as fillers affect how incident light interacts with free carriers.

3.2.4 Optical dielectric constant and energy loss functions of the blends

Both the real and imaginary parts of the optical dielectric constants, (ϵ_r and ϵ_i) along with the volume and surface energy loss functions (VELF and SELF) for a given blend are given by (El-naggar et al. 2023a, b, c):

$$\epsilon_r = n^2 - k^2 \quad (14)$$

$$\epsilon_i = 2nk \tag{15}$$

$$SELF = \frac{\epsilon_i}{(\epsilon_r + 1)^2 + \epsilon_i^2} \tag{16}$$

$$VELF = \frac{\epsilon_i}{\epsilon_r^2 + \epsilon_i^2} \tag{17}$$

A graph showing how the blend parameters ϵ_r , ϵ_i , VELF and SELF vary with wavelength is shown in Fig. 5. The ϵ_r and ϵ_i performances of the different blends, as expected, scale with their n and k values. In every blend, ϵ_r and VELF for each polymer are higher than ϵ_i and SELF. Doped blends have larger values for ϵ_r , ϵ_i , SELF and VELF than their undoped counterparts. Changes in ϵ_r and ϵ_i values could result from doping the blend with the fillers, which could alter the blend’s electrons’ interaction with light or alter the blend’s dipole motion (Wise 1998; Suma et al. 2017). The plots also demonstrated that the values of both the SELF and VELF functions rose as PANI was added and MnS concentration is increased in the nanocomposite, verifying that the increase in the number of defects was due to the fillers’ strong interaction with the blend matrix. A material’s optical response

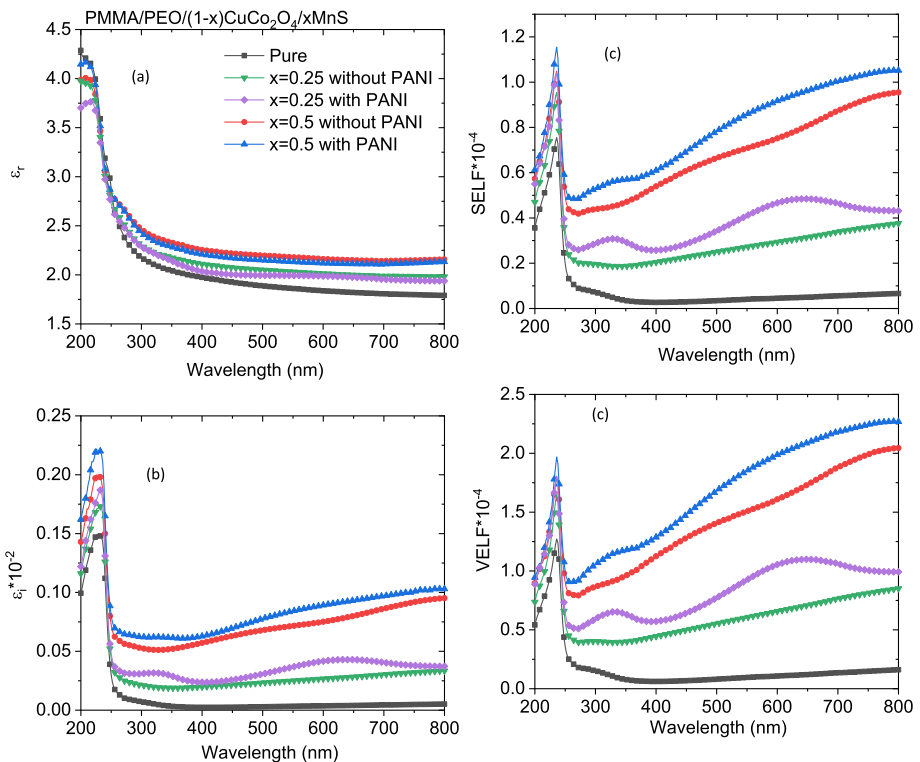


Fig. 5 The changes in **a** real and **b** imaginary dielectric constant, **c** SELF and **d** VELF with the wavelength for PMMA/PEO/(1-x)CuCo₂O₄/xMnS polymers with and without PANI

to the propagation of charge carriers through its electronic states in response to the excitation effect of incident electromagnetic wave energy is characterized by a parameter called the optical conductivity, σ_{opt} . It is an essential parameter in device fabrication because it describes the transitions electrons make between electronic states (Hendi and Rashad 2018).

3.2.5 Optical conductivity of the blends

Using its absorption coefficient spectrum and refractive index value, the following formula can be used to determine the spectral behavior of σ_{opt} (El-naggar et al. 2023a, b, c):

$$\sigma_{opt} = \frac{\alpha n C}{4\pi} \quad (18)$$

where C is velocity of the light.

For PMMA/PEO/(1-x)CuCo₂O₄/xMnS polymers with and without PANI, the σ_{opt} values appear to decrease with wavelength, as shown in Fig. 6. This reduction resembles the optical behavior of the absorption spectra and is indicative of the low transmittance of photons with low energies. There is a strong interaction between the nanocomposite/PANI and the blend, which causes an increase in optical conductivity as PANI is added and the MnS content in the nanocomposite is increased. This is because the number of free electrons grows as a consequence of the growth of defects (disorders).

3.3 Fluorescence analysis

Under an excitation wavelength of 317 nm, Fig. 7a displays the fluorescence (FL) spectra of PMMA/PEO/(1-x)CuCo₂O₄/xMnS blends with and without PANI. The graph demonstrated that the PMMA/PEO blend's FL spectrum covered a wide wavelength range, from 327 to 600 nm. Sub-peaks associated with UV-violets (347, 403, 420) nm, blue (469 nm), and yellow (573 nm) colors were found in the spectra. The $\pi \rightarrow \pi^*$ transition of PMMA carbonyl groups is responsible for the 573 nm sub-peak (Kara et al. 2020). Near-band emission (NBE) electron transformations give rise to UV and violet emissions, which have been linked to excitonic transitions. The blue color is due to luminescence emitted by defects (Heiba et al. 2016). It has been discovered by Xiong et al. (2001) that when PEO film is excited with $\lambda_{exc} = 400$ nm, PEO emits three excitation peaks (275, 320, and 360 nm) in the ultraviolet zone and one emission peak at about 410 nm, despite the fact that PEO in its natural state is not fluorescent. The fluorescent peaks of an unrefined polymer could

Fig. 6 Optical conductivity for PMMA/PEO/(1-x)CuCo₂O₄/xMnS polymers with and without PANI

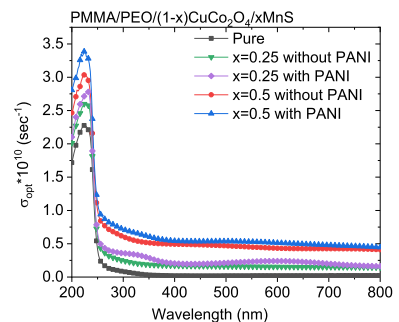
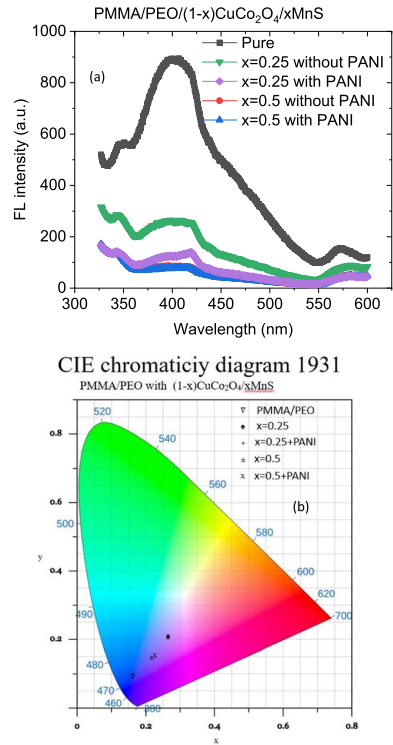


Fig. 7 **a** FL data and **b** CIE diagram for PMMA/PEO/(1-x)CuCo₂O₄/xMnS polymers with and without PANI



be the result of fluorescent impurities (Schreiber et al. 2014). Moreover, the luminescence efficiency and spectral position may alter as a consequence of interactions between the main chains or side chains of PMMA and PEO. Furthermore, in nonfluorescent polymers, discrete chromophores defined as "sub-fluorophores" may undergo space conjugation via cooperative intramolecular conformation followed by intermolecular aggregation, resulting in fluorescence or occasionally phosphorescence emission (Chatterjee et al. 2020). The FL intensity decreased after (1-x)CuCo₂O₄/xMnS was loaded into the PMMA/PEO blend, and it decreased even more as the quantity of MnS raised in the nanocomposite. As more PANI was added to the blend, the FL intensity dropped even further. PMMA/PEO's strong interaction with (1-x) CuCo₂O₄/xMnS and/or PANI may be to blame for this quenching.

Table 1 Direct and indirect optical band gap energies and chromaticity coordinates (x, y) for PMMA/PEO/(1-x)CuCo₂O₄/xMnS polymers with and without PANI

Sample	Direct E_g (eV)	Indirect E_g (eV)	CIE coordinates
PMMA/PEO	5.06	4.79	(0.1616, 0.0915)
PMMA/PEO with (1-x)CuCo ₂ O ₄ /xMnS			
x = 0.25	5.03	4.67	(0.2650, 0.2086)
x = 0.25 + PANI	4.99	4.62	(0.2640, 0.2043)
x = 0.5	4.91	4.58	(0.2158, 0.1494)
x = 0.5 + PANI	4.89	4.49	(0.2273, 0.1542)

This interaction generates trap sites through which excited electrons can be transferred (Li 2019). The doped blends that were studied could be used in photocatalytic reactions.

Normalized FL spectra are shown in Fig. 7a, and their chromaticity diagram in the 1931 standard (CIE) color space is shown in Fig. 7b to represent the samples' colors. Table 1 displays the CIE chromaticity coordinates (x , y) that correspond to each sample. Depending on the additives, the blends all displayed varying degrees of bluish-violet color.

3.4 Dielectric characteristics

3.4.1 Real and imaginary parts of the dielectric constant of the blends

PMMA/PEO/(1-x)CuCo₂O₄/xMnS blends with and without PANI are shown in Fig. 8a, b, displaying the real and imaginary parts of the dielectric constant (ϵ' , ϵ'') as a function of frequency at RT. The energy-storage capacity, denoted by the ϵ' value, can be thought of as a measure of the polarization of a fabricated dielectric. The tendency of dipoles in blended nanocomposite films to align themselves in the direction of the applied field causes a sharp increase in ϵ' at low frequencies.

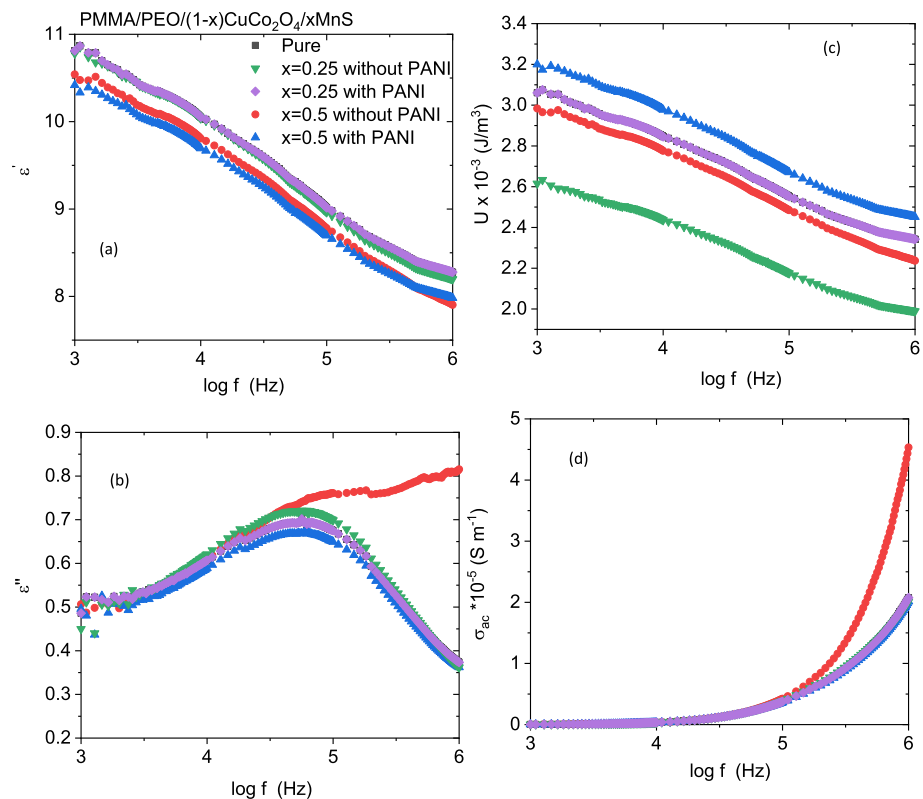


Fig. 8 The **a** real, **b** imaginary parts of the dielectric constant, **c** energy density and AC conductivity for PMMA/PEO/(1-x)CuCo₂O₄/xMnS polymers with and without PANI

Due to the charge's inability to follow the periodic reversal of the electrical field at high frequencies, the dielectric permittivity declines as a consequence of the charge's lag behind the applied field. The accumulation of charges reduces polarization, which in turn reduces ϵ' (Hafez et al. 2020). Minor changes in ϵ' were observed as PMMA/PEO blend was doped with nanocomposite containing 25% MnS with and without PANI. The nanocomposite's ϵ' diminished with rising MnS content and further declined with the addition of PANI. The interfacial polarization changed because the order distribution of PANI and nanocomposite in the PMMA/PEO film varied (Alzahrani et al. 2022b). Reduced space charge polarization relative to total polarization (Kalyani and Muthupandeeswari 2022) also contributes to a reduction in ϵ' . Doping PEO/PVA with MWCNTs/ZnO yielded similar outcomes (Alzahrani et al. 2022b). The non-Debye type of behavior (Alghamdi and Rajeh 2022) also contributes to the variation in the value of ϵ' by altering the density of charge carriers in the space charge accumulation area. As can be seen in Fig. 8b, the ϵ'' values of all films increased with increasing frequency until they peaked, after which they declined. The structural dynamics of the system are responsible for its relaxation peak. The nanocomposite's ϵ'' decreased as MnS content grew. In the corresponding polymer, the addition of PANI led to a further decrease in the value of ϵ'' .

3.4.2 Energy density of the blends

Using the next formula, one can determine the energy density (U), or the amount of energy that can be stored in a given volume of a material (Isasi et al. 1995):

$$U = \frac{1}{2} \epsilon_0 \epsilon' E^2 \quad (18)$$

where ϵ_0 and E are the permittivity of free space (8.85×10^{-12} F/m) and the electric field, respectively. U 's dependence on frequency for all blends is depicted in Fig. 8c. Doping the blend with nanocomposite samples and PANI resulted in a lower energy density, with the exception of the blend containing 50% MnS and PANI, where it rose.

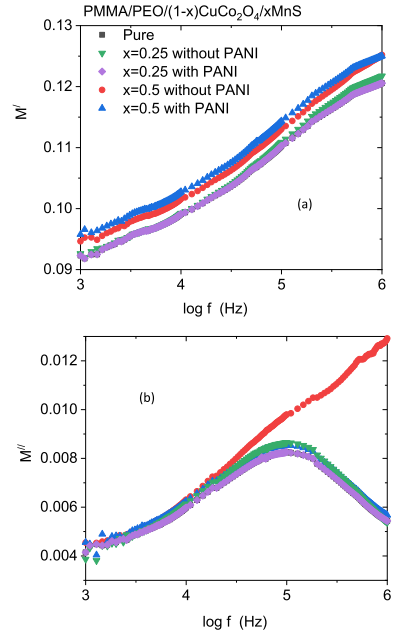
3.4.3 AC conductivity of the blends

The AC electrical conductivity, $\sigma_{ac}(\omega)$, plotted against $\ln f$ for all blends is shown in Fig. 8d. The AC conductivity spectra revealed a dispersion at high frequencies but a plateau (frequency independent) at lower frequencies. This trend is associated with a higher concentration of mobile ions in the blends (Taha and El-Nasser 2021). After adding the nanocomposite and/or PANI, the AC electrical conductivity of a pure PMMA/PEO film changed irregularly, reaching its maximum value as it was doped with 50% MnS. Similar results were observed for poly (vinyl butyral) nanocomposites films embedded with Co_3O_4 , CuO, NiO, TiO_2 , and Cr_2O_3 nanoparticles (Omer et al. 2022). Doping the host blend may have altered its ac conductivity by altering the defects on its surface, which in turn altered the interface polarization relaxation (Abdelhamied et al. 2022).

3.4.4 Electric modulus of the blends

The real M' and imaginary M'' components of the electric modulus and their frequency dependence are displayed for all samples in Fig. 9. These modulus spectra, which deliver a bulk response of the material, cancel out the effect of various unfavorable factors, such as

Fig. 9 The **a** real and **b** imaginary parts of electric modulus for PMMA/PEO/(1-x)CuCo₂O₄/xMnS polymers with and without PANI



electrode polarization. The M' of nanocomposite and/or PANI-loaded PMMA/PEO grew irregularly. It reached its peak performance after being loaded with 50% MnS and PANI. Each M'' spectrum displays a distinct relaxation peak, which is linked to the relaxation process (Khairy et al. 2020).

4 Conclusion

Phase identification analysis of (1-x)CuCo₂O₄/xMnS nanocomposite samples showed that all samples consisted of a single phase of CuCo₂O₄ with a cubic spinel structure. The transmission electron microscope technique confirmed the nanosized nature of the fillers. XRD confirmed the formation of different blends. Doping the PMMA/PEO blend with (1-x)CuCo₂O₄/xMnS increased the blend's absorbance. The blends' absorbance was also improved by PANI doping compared to blends without PANI. PMMA/PEO has a visible-range transmittance of roughly 89%. When the blend was loaded with a nanocomposite that consisted of 50% MnS and PANI, the transmittance dropped to 18%. Doping a PMMA/PEO blend with MnS led to increased reflectance in the visible spectrum, while loading the blend with PANI in addition decreased the reflectance. The optical band gap energies decreased as the blend was doped with nanocomposite, and they decreased even more as PANI was added. As the quantity of MnS in the nanocomposite raised, the n and k of the doped blend increased, but n decreased while k increased in the corresponding blend with PANI. Doped blends have a larger optical dielectric constant, energy loss function values and optical conductivity than their undoped counterparts. The values of both the SELF and VELF functions rose as PANI was added and MnS concentration is increased in the nanocomposite. All blends emitted UV-violet, blue and yellow colors. The FL intensity decreased after (1-x)CuCo₂O₄/xMnS was loaded into the PMMA/PEO blend, and it

decreased even more as the quantity of MnS was raised in the nanocomposite. As more PANI was added to the blend, the FL intensity dropped even further. The blends' dielectric constant and energy density diminished with rising MnS content and further declined with the addition of PANI. The AC electrical conductivity and electric modulus changed irregularly, reaching their maximum values as they were doped with 50% MnS.

Supplementary Information The online version contains supplementary material available at <https://doi.org/10.1007/s11082-023-05458-5>.

Acknowledgements The authors extend their appreciation to the Deputyship for Research & Innovation, Ministry of Education in Saudi Arabia for funding this research. (IFKSURC-1-1029).

Author contributions All authors have contributed, discussed the results and approved the final manuscript.

Funding This work is supported by the Deputyship for Research & Innovation, Ministry of Education in Saudi Arabia.

Data availability The authors confirm that the data supporting the findings of this study are available within the article.

Declarations

Conflict of interest The authors declare that they have no conflict of interest.

Ethical approval We agreed all terms and conditions for Ethics approval.

References

- Abdelhamied, M.M., Atta, A., Abdelreheem, A.M., Farag, A.T.M., El Okr, M.M.: Synthesis and optical properties of PVA/PANI/Ag nanocomposite films. *J. Mater. Sci. Mater. Electron.* **31**, 22629 (2020)
- Abdelhamied, M.M., Abdelreheem, A.M., Atta, A.: Influence of ion beam and silver nanoparticles on dielectric properties of flexible PVA/PANI polymer composite films. *Plast. Rubber Compos.* **51**(1), 1 (2022)
- Abdel-Kader, M.H., Mohamed, A.A.H., Almarashi, J.Q.M., Mohamed, M.B.: Investigating the tunable properties of double blended nanocomposite films exposed to direct Nd: YAG laser beam. *Opt. Mater.* **142**, 114100 (2023)
- Abdelrazek, E.M., Abdelghany, A.M., Badr, S.I., Morsi, M.A.: Structural, optical, morphological and thermal properties of PEO/PVP blend containing different concentrations of biosynthesized Au nanoparticles. *J. Mater. Res. Technol.* **44**, 132 (2017)
- Abed, A.N., Abed, R.N.: Characterization effect of copper oxide and cobalt oxide nanocomposite on poly(vinyl chloride) doping process for solar energy applications. *Prog. Color Colorants Coat.* **15**, 235 (2022)
- Abed, R.N., Kadhom, M., Ahmed, D.S., Hadawey, A., Yousif, E.: Enhancing optical properties of modified PVC and Cr2O3 nanocomposite. *Trans. Electr. Electron. Mater.* **22**, 317 (2021a)
- Abed, R.N., Yousif, E., Abed, A.R.N., Rashad, A.A., Hadawey, A., Jawad, A.H.: Optical properties of PVC composite modified during light exposure to give high absorption enhancement. *J. Non-Cryst. Solids* **570**, 120946 (2021b)
- Abed, R.N., Yousif, E., Abed, A.R.N., Rashad, A.A.: Synthesis thin films of poly(vinyl chloride) doped by aromatic organosilicon to absorb the incident light. *SILICON* (2022). <https://doi.org/10.1007/s12633-022-01893-3>
- Abutalib, M.M., Rajeh, A.: Influence of MWCNTs/Li-doped TiO2 nanoparticles on the structural, thermal, electrical and mechanical properties of poly (ethylene oxide)/ poly (methylmethacrylate) composite. *J. Organomet. Chem.* **918**, 121309 (2020)
- Albalawi, H., Alharbi, E.M., Al-Sulami, A.I., Al-Qahtani, N., Farea, M.O., Rajeh, A.: Synthesis and characterization of sodium alginate/polyvinyl alcohol/zinc oxide/iron oxide nanocomposites for electrochemical applications. *Polym. Compos.* **44**(3), 1762 (2023)

- Alghamdi, H.M., Rajeh, A.: Synthesis of $\text{CoFe}_2\text{O}_4/\text{MWCNTs}$ nanohybrid and its effect on the optical, thermal, and conductivity of PVA/CMC composite as an application in electrochemical devices. *J. Inorg. Organomet. Polym.* **32**, 1935 (2022)
- Alzahrani, E., Shaltout, A.A., Moustapha, M.E., Farea, M.O., Menazea, A.A.: Optical, structural, and electrical conductivity of PEO/chitosan incorporated with Se NPs produced by one-potential laser ablation. *J. Mater. Sci. Mater. Electron.* **33**, 12351 (2022a)
- Alzahrani, H.S., Al-Sulami, A.I., Alsulami, Q.A., Rajeh, A.: A systematic study of structural, conductivity, linear, and nonlinear optical properties of PEO/PVA-MWCNTs/ZnO nanocomposites films for optoelectronic applications. *Opt. Mater.* **133**, 112900 (2022b)
- Aziz, S.B., Nofal, M.M., Brza, M.A., Hussein, S.A., Mahmoud, K.H., El-Bahy, Z.M., Dannoun, E.M.A., Kareem, W.O., Hussein, A.M.: Characteristics of PEO incorporated with CaTiO_3 nanoparticles: structural and optical properties. *Polymers* **13**, 3484 (2021)
- Burba, C.M., Frech, R., Grady, B.: Stretched PEO-LiCF₃SO₃ films: polarized IR spectroscopy and X-ray diffraction. *Electrochim. Acta* **53**, 1548 (2007)
- Chatterjee, D.P., Pakhira, M., Nandi, A.K.: Fluorescence in “nonfluorescent” polymers. *ACS Omega* **5**, 30747 (2020)
- Choudhary, S.: Structural and dielectric properties of (PEO-PMMA)-SnO₂ nanocomposites. *Compos. Commun.* **5**, 54 (2017)
- El-Naggar, A.M., Heiba, Z.K., Kamal, A.M., Abd-Elkader, O.H., Mohamed, M.B.: Impact of ZnS/Mn on the structure, optical, and electric properties of PVC polymer. *Polymers* **15**(9), 2091 (2023a)
- El-naggar, A.M., Heiba, Z.K., Kamal, A.M., Mohamed, M.B.: Structural, dielectric, linear and nonlinear optical parameters of Zn_{0.9}Cu_{0.1}S filled PVA/CMC/PEG blends. *Opt. Quantum Electron.* **55**(9), 1 (2023b)
- El-naggar, A.M., Heiba, Z.K., Kamal, A.M., Mohamed, M.B.: The role of cobalt amount in ZnCdS nanofiller on the optical, thermal, dielectric and structure properties of PVA/PVP/PEG blends. *Opt. Quant. Electron.* **55**(7), 609 (2023c)
- El-naggar, A.M., Heiba, Z.K., Kamal, A.M., Mohamed, M.B.: Optical and dielectric behaviors of polyvinyl chloride incorporated with $\text{MgFe}_2\text{O}_4/\text{MWCNTs}$. *Diam. Relat. Mater.* **138**, 110243 (2023d)
- El-Shamy, A.G.: The optical anatomy of new polyvinyl alcohol/zinc peroxide (PVA/ZnO₂) nanocomposite films for promising optical limiting applications. *Prog. Org. Coat.* **150**, 105981 (2021)
- El-Sharnouby, M., El Askary, A., Awwad, N.S., Ibrahim, H.A., Moustapha, M.E., Farea, M.O., Menazea, A.A., Abdelghany, A.M.: Enhanced electrical conductivity and dielectric performance of ternary nanocomposite film of PEMA/PS/silver NPs synthesized by laser ablation. *J. Inorg. Organomet. Polym.* **32**, 2269 (2022)
- Farea, M.O., Alhadlaq, H.A., Alaizeri, Z.M., Ahmed, A.A.A., Sallam, M.O., Ahamed, M.: High performance of carbon monoxide gas sensor based on a novel PEDOT:PSS/PPA nanocomposite. *CS Omega* **7**(26), 22492 (2022)
- Hafez, R.S., Hakeem, N.A., Ward, A.A., Ismail, A.M., Abd El-kader, F.H.: Dielectric and thermal properties of PEO/PVDF blend doped with different concentrations of Li₄Ti₅O₁₂ nanoparticles. *J. Inorg. Organomet. Polym.* **30**, 4468 (2020)
- Hashim, A., Hadi, Q.: Synthesis of novel (polymer blend-ceramics) nanocomposites: structural: optical and electrical properties for humidity sensors. *J. Inorg. Organomet. Polym. Mater.* **28**, 1394 (2018)
- Heiba, Z.K., Mohamed, M.B., Imam, N.G., Mostafa, N.Y.: Optical and electrical properties of quantum composite of polyvinyl alcohol matrix with CdSe quantum dots. *Colloid Polym. Sci.* **294**(2), 357 (2016)
- Heiba, Z.K., Farag, N.M., El-naggar, A.M., Abdellatif, M., Aldhafiri, A.M., Mohamed, M.B.: Effect of Mo-doping on the structure, magnetic and optical characteristics of nano CuCo_2O_4 . *J. Mater. Res. Technol.* **10**, 832 (2021a)
- Heiba, Z.K., Mohamed, M.B., Badawi, A., Farag, N.M.: Effect of sulfur deficiency on the structural, optical and electronic properties of MnS nanostructures. *Chem. Phys. Lett.* **779**, 138877 (2021b)
- Heiba, Z.K., Mohamed, M.B., Farag, N.M., Ahmed, S.I.: Correlation between structural and optical characteristics upon changing the composition ratio of CuS@MnS nanocomposites. *Appl. Phys. A* **127**, 1 (2021c)
- Heiba, Z.K., Mohamed, M.B., Farag, N.M., Badawi, A.: Tracking the changes in the structural, optical and photoluminescent properties of $\text{CuCo}_2\text{O}_4/\text{MnS}$ nanocomposites with different composition ratios. *Z. Naturforschung A* **77**(3), 291 (2022)
- Heiba, Z.K., El-naggar, A.M., Kamal, A.M., Abd-Elkader, O.H., Mohamed, M.B.: Optical and dielectric properties of PVC/TiO₂/TBAI ionic liquid polymer electrolyte. *Opt. Mater.* **139**, 113764 (2023)
- Hendi, A.A., Rashad, M.: Photo-induced changes in nano-copper oxide for optoelectronic applications. *Physica B* **538**, 185 (2018)

- Isasi, J., López, M.L., Veiga, M.L., Ruiz-Hitzky, E., Pico, C.: Structural characterization and electrical properties of a novel defect pyrochlore. *J. Solid State Chem.* **116**, 290 (1995)
- Kafashan, H., Azizieh, M., Vatan, H.N.: Ultrasound-assisted electrodeposition of SnS: effect of ultrasound waves on the physical properties of nanostructured SnS thin films. *J. Alloy. Comp.* **686**, 962 (2016)
- Kalyani, P., Muthupandeewari, T.: Investigation on the altered properties of PVA filled magnesium oxide composite (PVA@xMgO) thin films. *Polym. Bull.* **79**, 10115 (2022)
- Kara, H., Oylumluoglu, G., Coban, M.B.: Photoluminescence properties of a new Sm(III) complex/PMMA electrospun composite fibers. *J. Clust. Sci.* **31**, 701 (2020)
- Khairy, Y., Elsaedy, H.I., Mohammed, M.I., Zahran, H.Y., Yahia, I.S.: Anomalous behaviour of the electrical properties for PVA/TiO₂ nanocomposite polymeric films. *Polym. Bull.* **77**, 6255 (2020)
- Koninck, M.D., Poirier, S.-C., Marsan, B.: CuxCo_{3-x}O₄ used as bifunctional electrocatalyst. *J. Electrochem. Soc.* **153**(11), A2103 (2006)
- Laourari, I., Lakhdari, N., Belgherbi, O., Medjili, C., Berkani, M., Vasseghian, Y., Golzadeh, N., Lakhdari, D.: Antimicrobial and antifungal properties of NiCu-PANI/PVA quaternary nanocomposite synthesized by chemical oxidative polymerization of polyaniline. *Chemosphere* **291**, 132696 (2022)
- Li, L.: Tunable memristic characteristics based on graphene oxide charge-trap memory. *Micromachines* **10**, 151 (2019)
- Liu, X., Sun, J., Liu, Y., Liu, D., Xu, C., Chen, H.: The CuCo₂O₄/CuO composite-based microspheres serve as a battery-type cathode material for highly capable hybrid supercapacitors. *J. Alloys Compd.* **894**, 162566 (2022)
- Mathela, S., Sangwan, B., Dhapola, P.S., Singh, P.K., Tomar, R.: Ionic liquid incorporated poly (ethylene oxide) (PEO) doped with potassium iodide (KI) solid polymer electrolyte for energy device. *Mater. Today: Proc.* **49**(8), 3250 (2022)
- McLure, D.S.: The distribution of transition metal cations in spinels. *J. Phys. Chem. Solids* **3**, 311 (1957)
- Mirmohseni, A., Wallace, G.G.: Preparation and characterization of processable electroactive polyaniline-polyvinyl alcohol composite. *Polymer* **44**, 3523 (2003)
- Morsi, M.A., El-Khodary, S.A., Rajeh, A.: Enhancement of the optical, thermal and electrical properties of PEO/PAM: Li polymer electrolyte films doped with Ag nanoparticles. *Phys. B: Condens. Matter* **539**, 88 (2018)
- Naidu, K.S., Palaniappan, S.: Formation of PANI-PVA salt via H-bonding between PVA and PANI: aqueous coating for electrostatic discharge, sensor and corrosion applications. *Sens. Int.* **1**, 100006 (2020)
- Ngai, K.S., Ramesh, S., Ramesh, K., Juan, J.C.: A review of polymer electrolytes: fundamental, approaches and applications. *Ionics* **22**, 1259 (2016)
- Omer, R.M., Al-Tikrity, E.T.B., Abed, R.N., Kadhom, M., Jawad, A.H., Yousif, E.: Electrical conductivity and surface morphology of PVB films doped with different nanoparticles. *Prog. Color Colorants Coat.* **15**, 191 (2022)
- Pei, Y., Liu, C., Han, Z., Neale, Z.G., Qian, W., Xiong, S., Jiang, Z., Cao, G.: Revealing the impacts of metastable structure on the electrochemical properties: the case of MnS. *J. Power. Sources* **431**, 75 (2019)
- Pereira, A.G.B., Paulino, A.T., Nakamura, C.V., Britta, E.A., Rubira, A.F., Muniz, E.C.: Effect of starch type on miscibility in poly(ethylene oxide) (PEO)/starch blends and cytotoxicity assays. *Mater. Sci. Eng. C* **31**, 443 (2011)
- Schreiber, M., Vivekanandhan, S., Cooke, P., Mohanty, A.K., Misra, M.: Electrospun green fibres from lignin and chitosan: a novel polycomplexation process for the production of lignin-based fibres. *J. Mater. Sci.* **49**, 7949 (2014)
- Sengwa, R.J., Dhatwarwal, P.: Polymer nanocomposites comprising PMMA matrix and ZnO, SnO₂, and TiO₂ nanofillers: a comparative study of structural, optical, and dielectric properties for multifunctional technological applications. *Opt. Mater.* **113**, 110837 (2021)
- Suma, G.R., Subramani, N.K., Shilpa, K.N., Sachhidananda, S., Satyanarayana, S.V.: Effect of Ce_{0.5}Zr_{0.5}O₂ nano fillers on structural and optical behaviors of poly(vinyl alcohol). *J. Mater. Sci. Mater. Electron.* **28**(14), 10707 (2017)
- Taha, T.A., El-Nasser, K.S.: Synthesis, thermal and dielectric investigations of PVDF/PVP/Co_{0.6}Zn_{0.4}Fe₂O₄ polymer nanocomposite films. *J. Mater. Sci. Mater. Electron.* **32**, 27339 (2021)
- Tanaka, K.: Optical properties and photoinduced changes in amorphous As-S films. *Thin Solid Films* **66**, 271 (1980)
- Wadkar, N.S., Waghuley, S.A.: Characterizing the electro-optical properties of polyaniline/poly(vinylacetate) composite films as-synthesized through chemical route. *Results Surf. Interfaces* **4**, 100016 (2021)
- Wang, R., Xu, H., Cheng, S., Liang, J., Gou, B., Zhou, J., Fu, J., Xie, C., He, J., Li, Q.: Ultrahigh-energy-density dielectric materials from ferroelectric polymer/glucose all-organic composites with a cross-linking network of hydrogen bonds. *Energy Storage Mater.* **49**, 339 (2022)

- Wise, D.L.: *Electrical and Optical Polymer Systems: Fundamentals: Methods, and Applications*. CRC Press, BocaRaton (1998)
- Wu, W., Ouyang, Q., He, L., Huang, Q.: Optical and thermal properties of polymethyl methacrylate (PMMA) bearing phenyl and adamantyl substituents. *Colloids Surf. A* **653**, 130018 (2022)
- Xiong, H.-M., Zhao, X., Chen, J.-S.: New polymer–inorganic nanocomposites: PEO–ZnO and PEO–ZnO–LiClO₄ films. *J. Phys. Chem. B* **105**, 10169 (2001)
- Yang, H., Zhou, J., Xu, H., Gou, B., Wang, R., Xie, C.: Achieving ultra-high discharge energy density of dielectric polymer nanocomposites by in situ synthesis. *Mater. Today Energy* **30**, 101165 (2022)

Publisher's Note Springer Nature remains neutral with regard to jurisdictional claims in published maps and institutional affiliations.

Springer Nature or its licensor (e.g. a society or other partner) holds exclusive rights to this article under a publishing agreement with the author(s) or other rightsholder(s); author self-archiving of the accepted manuscript version of this article is solely governed by the terms of such publishing agreement and applicable law.